Energy levels of Pr^{3+} ions in halide crystals

1992 J. Phys.: Condens. Matter 4 6141

(http://iopscience.iop.org/0953-8984/4/28/015)

J. Phys.: Condens. Matter 4 (1992) 6141–6154. Printed in the UK

Energy levels of Pr^{3+} ions in halide crystals

W A Hargreaves
1301 Poitras Drive, Vero Beach, FL 32963, USA

Received 23 December 1991, in final form 19 February 1992

Abstract. Energy levels of f–f transitions of Pr^{3+} ions in LaF_3, PrF_3 and $LaCl_3$ single crystals have been determined from optical absorption and emission studies at cryogenic temperatures. Older data are revised considerably, with strong changes in the energy-level positions of the $^1D_2$, $^3P_0$ and $^3P_1$ states.

1. Introduction

The energy-level system for the f^2 electrons of the Pr^{3+} ion is a comparatively simple one, and is almost completely revealed by optical absorption and emission studies of LaF_3:Pr^{3+} crystals. The purpose of the present paper is to present new experimental data which requires significant revisions of previously reported presentations.

2. Experimental details

The instrumentation for the measurements comprised a Perkin–Elmer 'Lambda 9' computer-controlled spectrometer, covering the spectral range from 185 to 3200 nm, for absorption measurements, and a McPherson model 218 computer-controlled stepper-motor, single-beam, multiple-grating spectrometer for absorption and emission measurements in all spectral ranges required. A Janis Research closed-cycle helium cryostat provided the crystal cooling system. The usual sample is a 6 mm polished cube with two opposing faces perpendicular to the LaF_3 crystal c axis. The sample is placed at the centre of two intersecting internal cavities, which are of 7×7 mm cross section and at right angles to each other, in the cryostat 'cold finger'. A 90° rotation of the cryostat permits observation of the directions both parallel and perpendicular to the c axis of the crystal. Crystal temperatures reach 8 K, as substantiated by the experimental fact that absorptions from the 57 cm^{-1} $^3H_4$ level to the $^1D_2$ and $^3P_1$ levels are essentially zero at the 8 K temperature, as predicted by Boltzmann statistics.

The symmetry of rare-earth doped LaF_3 crystals has been covered extensively in many published papers. The most recent x-ray work, by Cheetham *et al*, is discussed in a comprehensive coverage of symmetry relationships of rare-earth doped LaF_3 by Leavitt and Morrison [1]. The symmetry of Pr^{3+} sites in LaF_3 is C_2, and is such that the Pr^{3+} ion-site axes are at 120° to each other and the plane containing the C_2 axes is perpendicular to the LaF_3 crystal c axis. The transition-symmetry rules, quantized with respect to the C_2 site axes are as follows:

0953-8984/92/286141+14$04.50

C_2	A	B
A	π	σ
B	σ	π

When absorption is measured along the LaF_3:Pr^{3+} c axis, one observes strong π transitions of Pr^{3+}, with some weak σ transitions. The axes of the C_2 sites in this orientation of the crystal are in a plane with the source E vectors, and strong π excitation results, while there is only slight coupling of the E vectors with components of C_2 σ vectors. When absorption is measured in a direction perpendicular to the LaF_3:Pr^{3+} c axis, the Pr^{3+} transitions are strongly σ-like, with some weak π-like transitions. Here the E vectors of the source are much more strongly coupled to C_2 σ than to C_2 π. To a considerable extent, the crystal is self-polarizing.

All transition wavelengths are standard air values, and these are converted to energy values by means of tables. Energy values are rather accurate, since no wavelength was assigned to any transition unless a calibrating gas-emission line was concurrently recorded on the spectral trace involved. All data are the result of many repeated measurements, made on several instruments. They are accurate in the visible region to 0.4 Å, and in the infrared to 5 Å.

3. Results

The commonly used notation for doped crystals is used in the following text, such that LaF_3:$1Pr^{3+}$ represents a crystal of LaF_3 doped with one molar per cent PrF_3.

All of the crystal-field-split levels of Pr^{3+} ions in LaF:Pr^{3+} and PrF_3 crystals have been determined here by means of absorption studies, including the $^1S_0$ levels. In addition, there are interlocking confirmations involving emission transitions from higher excited levels to lower levels, similar to the work of Wong *et al* [2], Yen *et al* [3], Caspers *et al* [4], and many others.

To the limits of our experimental accuracy, there are no differences in the energy-level systems of LaF_3:$1Pr^{3+}$, LaF_3:$3Pr^{3+}$ and LaF_3:$10Pr^{3+}$. PrF_3, however, has a similar but somewhat different set of levels from LaF_3:Pr^{3+}, as discussed in various sections of this paper. All PrF_3 levels have been studied in absorption except those of $^3H_5$. Emission from the 20925 cm^{-1} level of PrF_3 to lower states has served to confirm and supplement the absorption data. Emission from the $^3P_1$ 20925 cm^{-1} level of PrF_3 (but as $^3P_0$') to $^3F_2$ and to $^3H_6$ has been reported by Allen [5]). Our experimental levels of LaF_3:Pr^{3+} and PrF_3 are listed in table 1.

3.1. The $^1D_2$ manifold

The electronic levels of $^1D_2$, detailed in table 1, differ considerably from previously reported results, since they are all in the energy region below 17000 cm^{-1}.

The $^1D_2$ energy region above 17000 cm^{-1} was studied in absorption for crystals of LaF_3:$1Pr^{3+}$ and LaF_3:$10Pr^{3+}$ at temperatures of 9 K, 20 K and 50 K to search for electronic transitions. It is concluded there is no evidence for the presence of $^1D_2$ electronic levels above 17000 cm^{-1}. In that spectral region, there are no indications of transitions that respond, with characteristic increases of transition intensity, as

Table 1. Experimental levels of Pr^{3+} in LaF_3 and PrF_3 crystals (in cm^{-1}).

	$LaF_3:Pr^{3+}$	PrF_3		$LaF_3:Pr^{3+}$	PrF_3		$LaF_3:Pr^{3+}$	PrF_3
$^1S_0$	46 966	46 946	$^1G_4$	10 501	10 511	$^3H_6$	4773	4780
				159	162		771	677
$^3P_2$	22 815	22 827		47	54		577	587
	731	732		35	44		554	529
	713	710		9998	9997		525	515
	686	695		909	907		498	498
	629	638		873	864		384	399
				748	735		329	335
$^1I_6$	21 682	21 697		713	699		301	307
	670	664					266	261
	650	617	$^3F_4$	7164	7179		243	241
	635	612		104	119		221	216
	605	566		30	46		163	149
	567	552		7000				
	551	522		6981	6996	$^3H_5$	2920	
	521	498		977			616	
	483	466		941	953		560	
	473	459		930			492	
	459	436		923	936		441	2453
	384	413					408	
	338	377	$^3F_3$	6719	6739		353	372
				619	637		304	311
$^3P_1$	21 006	21 010		597	615		274	282
	20 969	20 971		587	603		234	
	20 925	20 925		495	509		178	184
				487	506			
$^3P_0$	20 627	20 645		450	459	$^3H_4$	500	519
							337	310
$^1D_2$	16 903	16 902	$^3F_2$	5275	5296		297	261
	900	893		273	295		204	202
	895	880		198	216		195	145
	891	874		180	194		136	123
	872	872		134	150		78	88
							57	66
							0	0

the various levels of $^3H_4$ are increasingly populated when the crystal temperature is increased. Figure 1 shows the spectral region involved. The vertical tick bars in the lower left corner of the figure show the positions of the three electronic levels of Carnall *et al* [10] (three upper ticks), and the three electronic levels of Wong *et al* [2] (three lower ticks).

The electronic absorption spectra of $^1D_2$ are shown in figure 2. Listing the $^1D_2$ manifold transitions in ascending order of energy, the lines are: medium-strength 5925.4 Å π (16 872), weak 5918.7 Å π (16 891), strong 5917.3 Å π (16 895), and medium strength 5915.6 Å σ (16 900) and 5914.5 Å σ (16 903) lines.

The $^1D_2$ levels of PrF_3, listed in table 1, were determined in a similar way to the above, but have somewhat different energy values: medium-strength 16 872, medium-strength 16 874, weak 16 880, weak 16 893, and very strong 16 902. Transitions involving $^3H_4$ levels above the zero-energy level of PrF_3 are very different from those of $LaF_3:Pr^{3+}$, since the $^3H_4$ levels are strongly different.

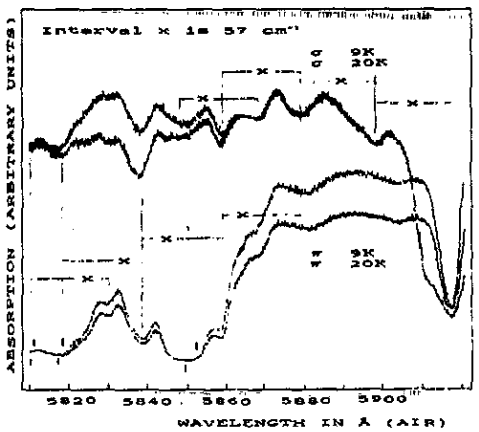

Figure 1. Absorptions $^3H_4$ to $^1D_2$ of LaF_3:10Pr^{3+} in the phonon region above 17 000 cm^{-1} at 9 K and 20 K. Upper traces, σ (with a 7 mm path perpendicular to c); lower traces, π (with a 7 mm path parallel to c).

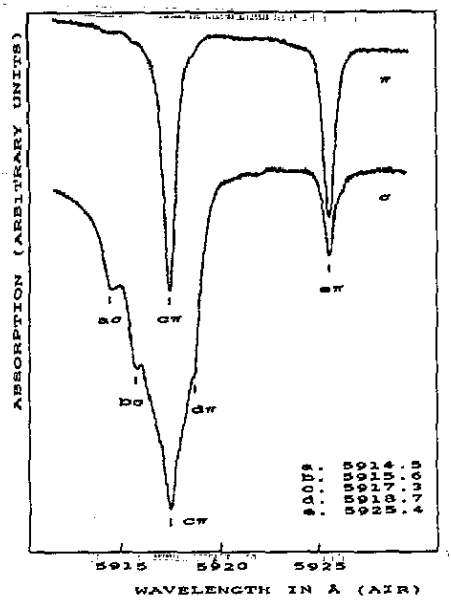

Figure 2. Absorptions $^3H_4$ to $^1D_2$ in the electronic region of LaF_3:1Pr^{3+} at 9 K. Upper trace, π (with a 7 mm path parallel to c); lower trace, σ (with a 7 mm path perpendicular to c).

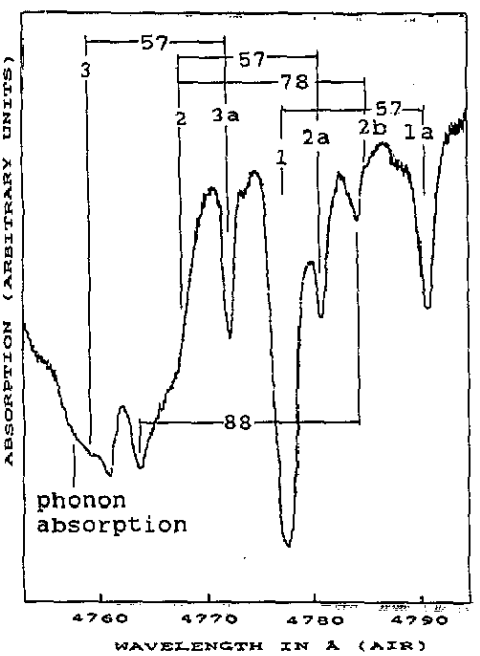

Figure 3. Absorptions $^3H_4$ to $^3P_1$ in the electronic region of LaF_3:3Pr^{3+} for a 15 mm path at an average temperature of about 20 K. The random orientation shows both π and σ absorptions.

3.2. The $^3P_1$ manifold

Another difference between this paper and other reported data is in the identification of the 20 925 cm^{-1} level as being the lowest level of the $^3P_1$ manifold, rather than a single-level $^3P_0$ state at 20 925 cm^{-1}. The basis for this new identification lies in data (such as figure 3) which show the $^3H_4$ to $^3P_1$ absorptions of LaF_3:3.0 Pr^{3+} at 20 K. The transitions from $^3H_4$ (0, 57 and 78 cm^{-1}) to the $^3P_1$ levels (21 006, 20 969 and 20 925 cm^{-1}) are identified in the figure.

Table 2. Predicted absorption and emission transitions between the levels of $^3H_4$ and the $^3P_0$ and $^3P_1$ levels (calculated from measured values). All listed transitions between $^3H_4$ and $^3P_1(1)$ (20 925) have been observed experimentally, as well as many of the other predicted transitions between $^3H_4$ and $^3P_1(2)$, $^3P_1(3)$, and $^3P_0(0)$ in the table. Figures 3, 7(*a*) and 7(*b*) show some of the latter experimental transitions. Observed emission transitions from $^3P_0$ to $^3H_4$ are shown in parentheses.

			$^3H_4$ (cm^{-1})								
$LaF_3:Pr^{3+}$			0	57 a	78 b	136 c	195 d	204 e	297 f	337 g	500 h
$^3P_1$ (cm^{-1})	(3)	21 006	4759.2	4772.2	4777.0	4790.3	4803.9	4805.9	4827.5	4836.9	4875.3
	(2)	20 969	4767.6	4780.6	4785.5	4798.8	4812.4	4814.5	4836.2	4845.5	4884.1
	(1)	20 925	4777.7	4790.7	4795.6	4808.9	4822.6	4824.7	4846.5	4855.9	4894.7
$^3P_0$ (cm^{-1})	(0)	20 627	4846.7	4860.1	4865.1	4878.9	4893.0	4895.1	4917.5	4927.2	4967.2
				(4860)	(4865)				(4917)	(4927)	(4967)
			$^3H_4$ (cm^{-1})								
PrF_3			0	66 a	88 b	123 c	145 d	202 e	261 f	310 g	519 h
$^3P_1$ (cm^{-1})	(3)	21 010	4758.3	4773.3	4778.4	4786.4	4791.4	4804.5	4818.2	4829.6	4878.9
	(2)	20 971	4767.2	4782.2	4787.3	4795.3	4800.4	4813.6	4827.3	4838.7	4888.2
	(1)	20 925	4777.7	4792.8	4797.9	4805.9	4811.0	4826.1	4838.0	4849.5	4899.2
$^3P_0$ (cm^{-1})	(0)	20 645	4842.5	4858.0	4863.2	4871.5	4876.7	4892.3	4904.5	4916.3	4967.4
				(4858)	(4864)	(4870)	(4876)				

Table 2 lists all predicted and observed transitions between $^3H_4$ and $^3P_1$, and also between $^3H_4$ and $^3P_0$. The $^3P_0$ energy level is discussed later in the paper.

Support for the new $^3P_1$ energy position is provided by the experimental strengths of emission transitions of $LaF_3:Pr^{3+}$ from the lowest $^3P_1$ level (20 925 cm^{-1}) to lower states. All of these emission transitions which are sufficiently strong to be observed by our methods are listed as follows (and recorded in table 3):

very strong to $^3H_4$	strong to $^3H_5$	strong to $^3H_6$
medium to $^3F_2$	weak to $^3F_3$	medium to $^3F_4$.

There are transitions from $^3P_1$ (J odd) to terminal states with both odd and even J values. Judd–Offelt intensity selection rules [6, 7] predict weak or no transitions between $J = 0$ and $J =$ odd manifolds, and are completely operative in the emission transitions from $^1S_0$ to lower states, as shown in a later section of this paper.

Figures 4(*a*) and (*b*) show the emission of LaF_3:10Pr^{3+} at 10 K from $^3P_1$ 20 925 cm^{-1} to $^3H_4$ when the crystal is optically pumped with energy just above the $^3P_1$ manifold. The strengths of all emission transitions increase greatly as the

Table 3. Emission from $^3P_1$ and $^1D_2$ of $LaF_3:Pr^{3+}$ to lower states.

Absorption from $^3H_4(0)$		Emission from $^3P_1$ (20 925 cm^{-1})		Emission from $^1D_2$ (16 872 cm^{-1})		Emission from $^1D_2$ (16 895 cm^{-1})	
(cm^{-1})		Calc. (Å)	Obs. (Å)	Calc. (Å)	Obs. (Å)	Calc. (Å)	Obs. (Å)
$^3H_5$	2920	5552.5		7165.5	7167		
	2616	5460.3		7014.6	7015		
	2492	5423.6		6952.2			
	2441	5408.6	5408.6	6927.6	6928		
	2408	5398.9	5399.5	6911.8			
	2353	5382.9	5382.8	6885.6	6887		
	2304	5368.8	5368.9	6862.5			
	2274	5360.1	5360.2	6848.4	6850		
	2234	5348.7	5348.6	6829.6	6832		
	2180	5333.3	5332.5	6804.5	6805		
	2178	5332.7	5332.5	6803.6	6804		
$^3H_6$	4763	6185.7	6186.3	8256.0	8257		
	4671	6150.6	6149.9	8193.7	8195		
	4577	6115.3	6115.5	8131.1	8131		
	4554	6106.7	6106.1	8115.9			
	4525	6095.9	6094.8	8096.8			
	4498	6085.8	6088.3	8079.2	8078		
	4384	6043.9	6045.2	8005.4			
	4329	6023.8		7970.3			
	4301	6013.7	6013.9	7952.5			
	4266	6001.1	6000.8	7930.4	7932		
	4243	5992.8		7916.0			
	4221	5984.9	5984.5	7902.2		7888.0	7890
	4163	5964.2		7866.1			
$^3F_2$	5275	6388.1	6388.7	8620.6	8619.2	8603.6	8604.2
	5273	6387.3	6388.7	8619.1	8619.2	8602.1	8604.2
	5198	6356.8	6357.6	8563.7	8563.2	8546.9	8547.7
	5180	6349.5	6350.3	8550.6	8547.7	8533.8	8533.8
	5134	6331.0	6331.4	8517.0	8516.7	8500.4	8500.7
$^3F_3$	6719	7037.4	7038				
	6619	6988.2					
	6597	6977.4					
	6587	6972.6	6972				
	6495	6928.1	6928				
	6487	6924.3					
	6450	6906.6	6906				
$^3F_4$	7164	7264.9	7265				
	7104	7233.4	7233				
	7030	7194.8	7195				
	7000	7179.3	7179				
	6981	7169.5	7169				
	6977	7167.5					
	6942	7149.5	7150				
	6930	7143.4					
	6923	7139.8					

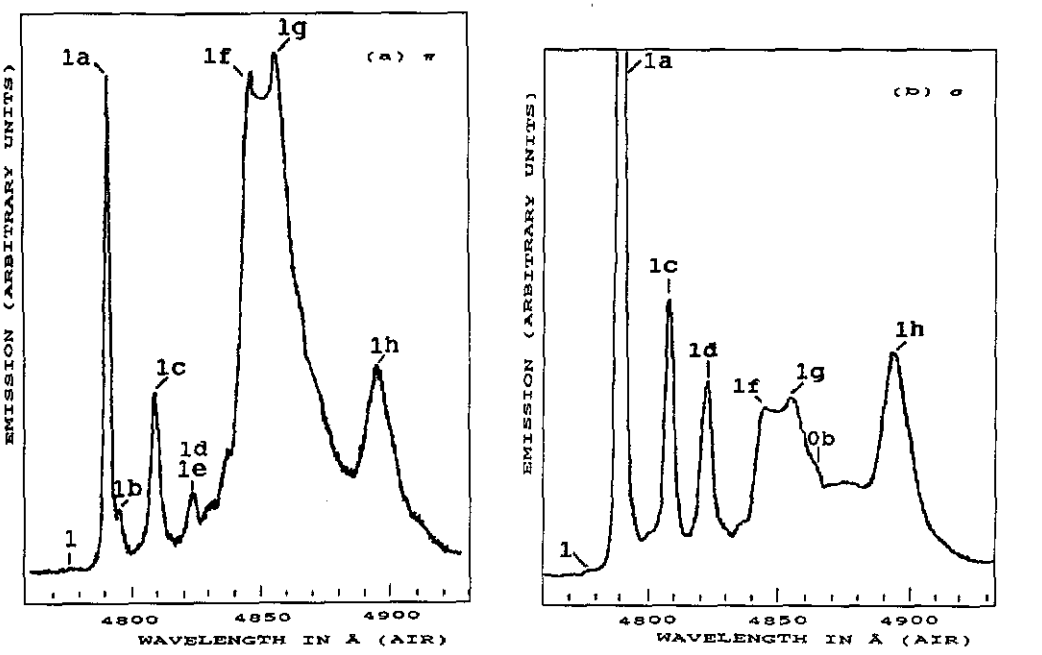

Figure 4. (*a*) Emission $^3P_1$ to $^3H_4$ of F_3:10Pr^{3+} at 9 K resulting from optical pumping at 4598 Å from the side. Polarization π, observed for a 4 mm path along *c*. (*b*) Emission $^3P_1$ to $^3H_4$ of LaF_3:10Pr^{3+} at 9 K resulting from optical pumping at 4598 Å from the side. Polarization σ, observed for a 4 mm path perpendicular to *c*.

crystal temperature is decreased below 20 K. As the crystal temperature is lowered below 15 K, the $^3H_4$ 57 cm^{-1} level depopulates rapidly, and the 20 925 to 57 cm^{-1} emission becomes dominantly the strongest of all.

In table 3 the energies of emission from $^3P_1$ (and from $^1D_2$) to levels of lower states are in excellent agreement with the absorption-derived level data for those lower levels. Both sets of data, absorption and emission, were obtained independently of each other.

3.3. The $^1I_6$ manifold

The energy-state system for isolated free ions of Pr^{3+}, as developed by Sugar [8] and Crosswhite *et al* [9], place the $^3P_1$ state at 22 008 cm^{-1}, closely below the $^1I_6$ state at 22 212 cm^{-1}. Previous published solutions for the levels of Pr^{3+} in crystals have also assigned a $^3P_1$ level position near the levels of the $^1I_6$ state, but those solutions are contradicted by various results in this paper.

Table 4 lists the 13 levels of $^1I_6$, as determined from $^3H_4$ to $^1I_6$ absorption measurements, and from $^1S_0$ to $^1I_6$ emission transitions. This defines the $^1I_6$ energy-level span. The observed transitions from $^1S_0$ to $^1I_6$ are indicated in figure 5 by arrows to the pertinent levels. Wong *et al* [2] place $^3P_1$ at the lower-energy end of the $^1I_6$ spectrum; their lowest level in the region is 21 469.8 cm^{-1}. Our lowest $^1I_6$ level at 21 338 cm^{-1} is clearly confirmed by an emission of wavelength 3900.9 Å from $^1S_0$ to 21 338 cm^{-1}. The Wong *et al* '$^3P_1$' levels are above the 21 338 level, are $^1I_6$ levels in table 1, and involve terminal levels of $^1S_0$ to $^1I_6$ emission transitions, as in table 4 and figure 5. Transitions from $^1S_0$ to $^3P_1$ are forbidden. The data of Carnall

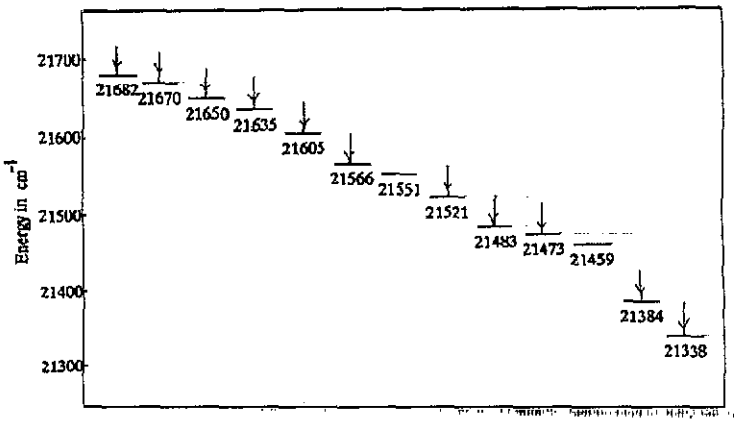

Figure 5. Observed emission (arrows) from $^1S_0$ at 46 966 cm^{-1} of LaF_3:1Pr^{3+} at 9 K. The levels of $^1I_6$ are taken from tables 1 and 4.

et al [10] similarly defines 21 458 cm^{-1} as a $^3P_1$ level, but that transition is a weak absorption inside the span of proven $^1I_6$ levels in figure 5.

Table 4. Emission of $^1S_0$ LaF_3:Pr^{3+} at 46 966 cm^{-1} to lower states. Calculated values are determined from the experimental value of $^1S_0$ (46 966 cm^{-1}), measured in absorption, and the energies of the terminal states, also measured in absorption.

$^3F_4$	$^1S_0$ to $^3F_4$		$^1G_4$	$^1S_0$ to $^1G_4$		$^1I_6$	$^1S_0$ to $^1I_6$	
(cm^{-1})	Calc. (Å)	Obs. (Å)	(cm^{-1})	Calc. (Å)	Obs. (Å)	(cm^{-1})	Calc. (Å)	Obs. (Å)
7164	2511.6	2512.0	10 501	2741.6	2741.9	21 682	3954.0	3954.1
7104	2507.9	2508.4	10 159	2716.1	2715.9	21 670	3952.1	3952.1
7030	2503.2	2503.7	10047	2707.8	2707.5	21 650	3949.0	3949.0
7000	2501.3		10035	2707.0		21 635	3946.6	3946.6
6981	2500.1		9998	2704.2		21 605	3942.0	3941.7
6977	2499.8		9909	2697.7	2698.3	21 566	3935.9	3936.0
6942	2497.7		9873	2695.1		21 551	3933.6	
6930	2497.0		9748	2686.1	2686.2	21 521	3928.9	3929.3
6923	2496.5		9713	2683.5		21 483	3923.1	3923.0
						21 473	3921.5	3921.5
						21 459	3919.4	
						21 384	3907.9	3907.9
						21 338	3900.9	3900.9

3.4. Transitions involving the $^1S_0$ state

The energy of the single level $^1S_0$ of the f^2 state of LaF_3:Pr^{3+} was determined by Carnall *et al* [10] as 46 986 cm^{-1}; this was confirmed by Elias *et al* [11]. Using three-photon excitation, Yen *et al* [12] determined an energy of 46 965 cm^{-1} for $^1S_0$, and Cordero-Montalvo and Bloembergen [13], with two-photon excitation, found a value of 46 990 cm^{-1}, but corrected this to 46 961 ±5 cm^{-1} in 1985 [14].

The absorption transitions from $^3H_4$ levels to the $^1S_0$ level in LaF_3:Pr^{3+} and PrF_3 are readily available to one-photon spectroscopy, although the transitions are weaker than transitions to most other states. In carefully calibrated absorption spectra we

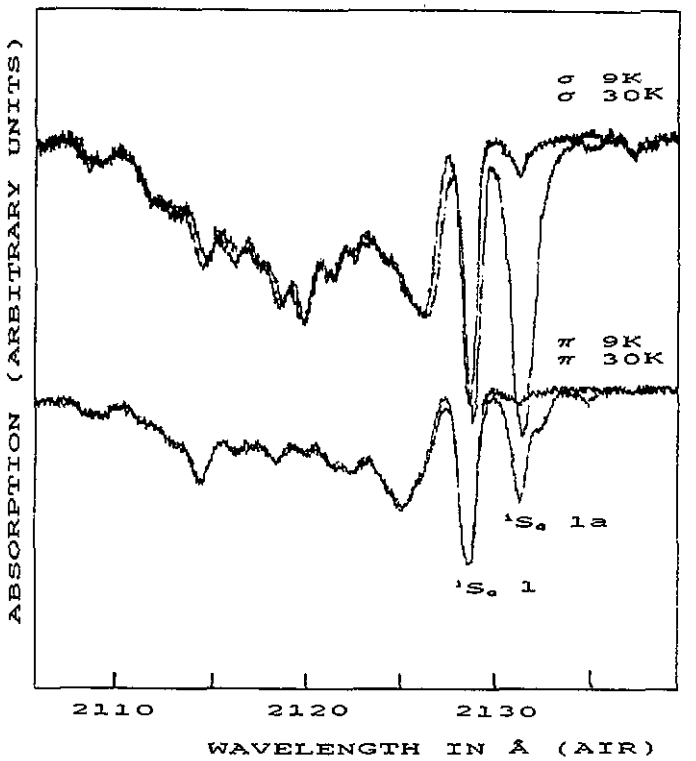

Figure 6. Absorptions $^3H_4$ to $^1S_0$ of LaF_3:10Pr^{3+} at 9 K and 30 K. Upper trace, π (with a 7 mm path parallel to c); lower trace, σ (with a 7 mm path perpendicular to c).

have measured the transition energy from $^3H_4$ to $^1S_0$ as 46 966±2 cm^{-1} for all Pr^{3+} dopings from 1 to 10 mol%. In PrF_3 the $^1S_0$ energy value is 46 946±2 cm^{-1}. Figure 6 shows the low-temperature absorption spectrum of $^1S_0$ in LaF_3:10Pr^{3+}.

As demonstrated by Elias *et al* [11], strong emission transitions from $^1S_0$ to lower states arise when the $^1S_0$ state of LaF_3:Pr^{3+} is optically pumped. Our measurements of such transitions are listed in table 4 (the terminal levels were accurately measured and calibrated in absorption, and are listed in table 1); the agreement between calculated and observed emission wavelengths confirms the levels determined in absorption. In particular, table 4 is a many-fold confirmation of the absorption-measured $^1S_0$ level at 46 966 cm^{-1}.

The pumping of $^1S_0$ was accomplished with a water-cooled deuterium lamp with a MgF_2 exit window, and therefore the lamp would pump into higher-configuration bands of Pr^{3+} at wavelengths below 2000 Å, as well as directly into $^1S_0$. However, similar emissions from $^1S_0$ were observed (at much lower intensities) when an interference filter with 15% peak transmission at 2000 Å was inserted into the pumping beam. Most of the pumping energy in this case was just above the $^1S_0$ energy level.

Scanning the emission energy spectrum from the $^1S_0$ energy downwards, the first observation is of very weak unresolved transitions to $^3H_4$. Next are very weak transitions to $^3H_6$ (~ 2350 Å); very weak transitions to $^3F_2$ (~ 2390 Å); strong transitions to $^3F_4$ (~ 2510 Å); very strong transitions to $^1G_4$ (~ 2715 Å); weak transitions to $^1D_2$ (~ 3350 Å); very strong transitions to $^1I_6$ (~ 3990 Å); and finally, as the last of the emission transitions from $^1S_0$ to lower states, very weak transitions

to $^3P_2$ (~ 4123 Å). All $J(0)$ to J(even) transitions are seen in the emission spectra from $^1S_0$; no transitions to J(odd) appear.

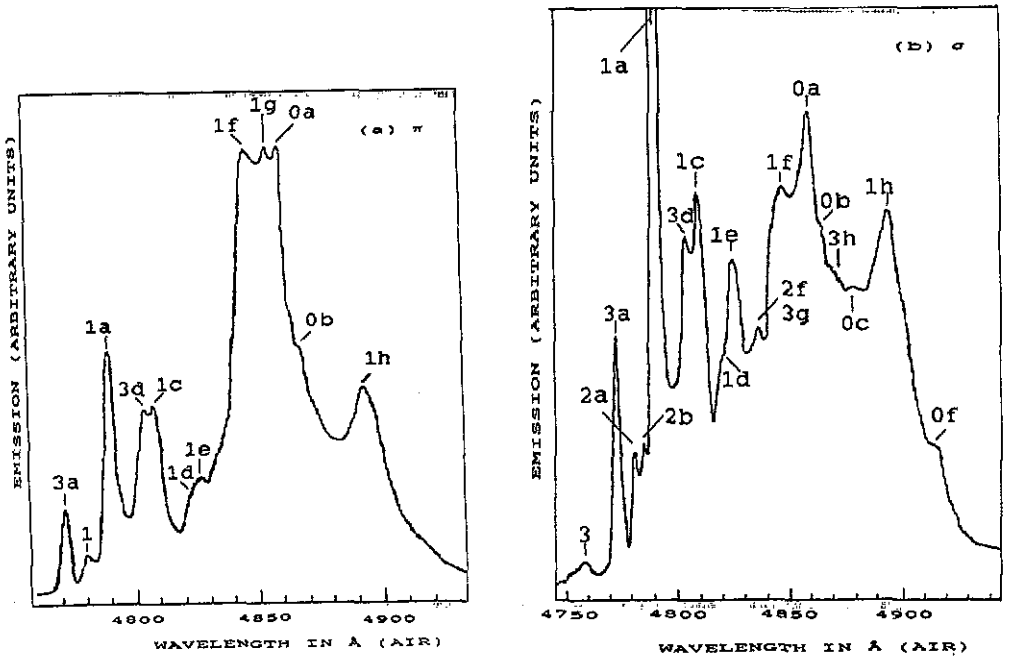

Figure 7. Emissions $^3P_1$, $^3P_0$ *to* $^3H_4$ *of* LaF_3:$10Pr^{3+}$ *at 9 K, resulting from optical pumping from the side with narrow-band energy in the* $^1S_0$ *energy region. (a) Polarization* π, *observed for a 4 mm path along c. (b) Polarization* σ, *observed for a 4 mm path perpendicular to c.*

In addition to producing transitions from $^1S_0$ to lower levels, as discussed above, the pumping of the LaF_3:Pr^{3+} $^1S_0$ level results in other, unexpected emission transitions. As seen in figures 7(*a*) and (*b*), emission is observed from all levels of $^3P_1$ to the levels of $^3H_4$, not just from the $^3P_1$ 20 925 cm^{-1} lowest level. Also, medium-strength emission from 20 925 cm^{-1} to levels of $^3H_5$ and $^3H_6$ is observed. These emissions from $^3P_1$ appear both with and without the 2000 Å pump filter (referred to above) and so are the result of direct pumping into the $^1S_0$ level. Figures 7(*a*) and (*b*) give evidence of transitions from $^3P_1(3)$ at 21 006 cm^{-1}, and from $^3P_1(2)$ at 20 969 cm^{-1}, to various $^3H_4$ levels, as well as transitions from $^3P_1(1)$ at 20 925 cm^{-1} to all the levels of $^3H_4$. Table 2 shows the transitions involved and the method of denoting particular transitions in the various figures of the paper (e.g. 3a is the transition from $^3P_1(3)$ at 21 006 cm^{-1} to $^3H_4(a)$ at 57 cm^{-1}).

Emission transitions from $^1S_0$ to $^3P_1$ are not allowed, but there is apparently a coupling between $^1S_0$ and $^3P_1$ which energizes the $^3P_1$ state and produces emission transitions from the three levels of $^3P_1$ to $^3H_4$. In this process, it appears that fast non-radiative phonon transitions from the upper two levels of $^3P_1$ to the 20 925 cm^{-1} level are considerably reduced when the remote $^1S_0$ level is pumped to produce emission from $^3P_1$.

3.5. The $^3P_0$ state

The $^3P_0$ level is close in energy to the levels of $^3P_1$, and, as a consequence, the

absorption and emission transitions of the two states are intermingled. The weak strength of transitions between $^3P_0$ and $^3H_4$ (like those between $^1S_0$ and $^3H_4$), the forbidden transition from $^3P_1$ to $^3P_0$, and the intermingling of $^3P_1$ and $^3P_0$ transitions are reasons why the $^3P_0$ state has not previously been located correctly. However, emission from $^3P_0$ to $^3H_4$ has been observed in the present study, as can be seen in figures 7(*a*) and (*b*) and table 2. Weak emission from $^3P_0$ to $^3F_2$ has also been observed.

3.6. Transitions of Pr^{3+} ions in $LaCl_3$:Pr^{3+}

Accommodation of the data obtained in the LaF_3:Pr^{3+} and PrF_3 systems with results in other Pr^{3+}-doped crystals is a pertinent subject. A previous paper on the energy levels of Pr^{3+} ions in CaF_2 single crystals is consistent in general with the present paper regarding the energy position of the ^3P manifolds [15]. That paper also suggested revisions to the accepted energy-level model for Pr^{3+} ions in $LaCl_3$, based on the experimental results for CaF_2:Pr^{3+}.

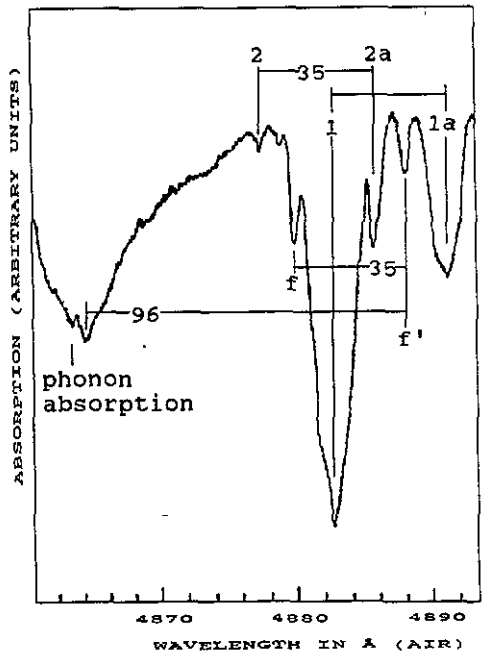

Figure 8. Absorptions $^3H_4$ to $^3P_1$ of $LaCl_3$:$2Pr^{3+}$ at 20 K. Absorptions f and f' are apparently related to phonon-assisted levels, similar to those in the absorption region $^3H_4$ to $^3P_1$ of LaF_3:Pr^{3+}.

In addition to the work on LaF_3:Pr^{3+} a rather complete study of optical absorption and emission has been made on $LaCl_3$:Pr^{3+}. The results confirm the most recent paper of Rana *et al* [16], except for the positions of the ^3P and $^1I_6$ manifolds. Figure 2 of [15] should be revised to conform to the Rana μ values, in particular, $^3H_4$ (0 cm^{-1}) is correctly $\mu = 2$. The energy values of $^3P_1$, as given in [15], are to be corrected as per table 5 of the present paper. However, [15] is correct in its (approximate) identification of the $^1I_6$ levels, and in its new positioning of the ^3P

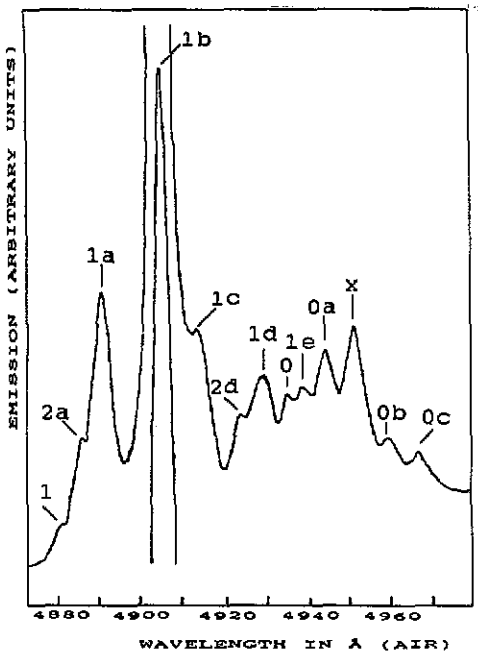

Figure 9. Emissions $^3P_1$ and $^3P_0$ to $^3H_4$ of $LaCl_3$:$2Pr^{3+}$ at 20 K. Labelling notation identifying the emissions as in table 5.

Table 5. Emission from $^3P_1$ and $^3P_0$ levels of $LaCl_3$:Pr^{3+} to $^3H_4$ levels.

Levels	cm^{-1}	$^3H_4$	0, $\mu = 2$	34, $\mu = 3$	96, $\mu = 2'$	132, $\mu = 3'$	192, $\mu = 1$	228, $\mu = 0$
$^3P_1(2)$	20498	$\mu = 1$	4877.2	4885.2	4900.2	4908.8	4923.4	4932.1
			2	2a[a]	2b	2c	2d[a]	2e[b]
$^3P_1(1)$	20475	$\mu = 0$	4882.7	4890.8	4905.7	4914.4	4928.9	4937.7
			1[a]	1a[a]	1b[a]	1c[a]	1d[a,b]	1e[a,b]
$^3P_0$	20259	$\mu = 0$	4934.8	4943.1	4958.3	4967.2	4982.0	4991.0
			0[a]	0a[a]	0b[a]	0c[a]	0d[b]	0e[b]

[a] See figure 9.
[b] Transitions forbidden by $C3_h$ rules. The reason for the presence of transitions 1d and 1e is unknown.

manifolds (see note added in proof). The evidence is apparent in figures 8 and 9 of this paper, which show the $^3P_1$ absorption and emission with respect to $^3H_4$ levels.

As in the LaF_3:Pr^{3+} analysis, the position of $^3P_0$ is identified in $LaCl_3$:Pr^{3+} by the emission data of figure 9, and table 5, which summarize the results for the $^3P_1$ and $^3P_0$ states of $LaCl_3$:Pr^{3+}.

4. Conclusion

A considerable amount of the physics literature involves the fitting of experimental Pr^{3+} f^2 levels, in many different crystal hosts, to a free-ion energy-level system, and to a point-charge crystal-field model. The fitting procedure has involved an increasing

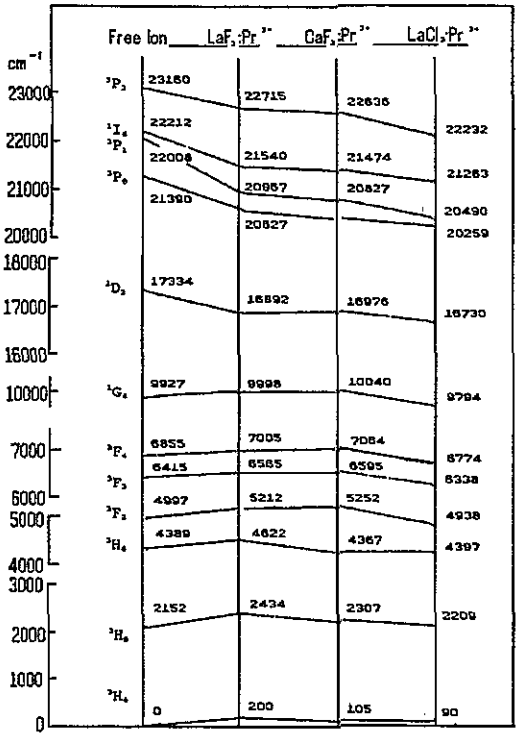

Figure 10. Schematic representation of Pr^{3+} states in halide crystals.

number of parameters, as the knowledge of interaction involvement has developed [17]. The evaluation of such interactions requires expertise beyond the scope of the present paper. The experimental data of this paper will aid further theoretical work. Figure 10 is a schematic representation of our results.

Note added in proof. Over the past 20 years many papers have been published which show that the single-ion, F^{-1}-compensated, tetragonal site of CaF2:Pr^{3+} is a weak site, especially in crystals with dopings of over 0.1 molar percent Pr^{3+} concentration. The structure of strong doping concentrations is dominated by 'cluster sites', which are multiple pairings of the F^{-1}-compensated Pr^{3+} single ion, as is made evident by considerably different crystal-field splittings and non-tetragonal spectra. The experimental results in Hargreaves' paper [15] on the optical spectra of CaF_2:Pr^{3+} represent this latter structure and not the single-ion tetragonal structure.

References

[1] Leavitt R P and Morrison C A 1980 *J. Chem. Phys.* **73** 749
[2] Wong E Y, Stafsudd O M and Johnston D R 1963 *J. Chem. Phys.* **39** 786
[3] Yen W M, Scott P L and Schawlow A L 1964 *Phys. Rev.* A **136** 271
[4] Caspers H H, Rast H E and Buchanan R A 1965 *J. Chem. Phys.* **43** 2124
[5] Allen J W 1975 *Phys. Rev. Lett.* **35** 128
[6] Judd B R 1962 *Phys. Rev.* **127** 750
[7] Offelt G S 1962 *J. Chem. Phys.* **37** 511
[8] Sugar J 1965 *J. Opt. Soc. Am.* **55** 1058
[9] Crosswhite H M, Dieke G H and Carter W J 1965 *J. Chem. Phys.* **43** 2047

[10] Carnall W T, Fields P R and Sarup R 1969 *J. Chem. Phys.* **51** 2587
[11] Elias L R, Heaps W S and Yen W M 1973 *Phys. Rev.* B **8** 4989
[12] Yen W M, Levey C G, Huang S and Lai S T 1981 *J. Lumin.* **24–25** 659
[13] Cordero-Montalvo C D and Bloembergen N 1984 *Phys. Rev.* B **30** 438
[14] Cordero-Montalvo C D and Bloembergen N 1985 *Phys. Rev.* B **31** 613
[15] Hargreaves W A 1972 *Phys. Rev.* B **6** 3417
[16] Rana R S and Kaseta F W 1983 *J. Chem. Phys.* **79** 5280
[17] Judd B R, Crosswhite H H and Crosswhite H 1969 *J. Chem. Phys.* **169** 130